Electrochemical Evaluation of a Napthalene Diimide Derivative for Potential Application in Aqueous Organic Redox Flow Batteries

(article starts on next page)

Electrochemical Evaluation of a Napthalene Diimide Derivative for Potential Application in Aqueous Organic Redox Flow Batteries

Cedrik Wiberg, Francis Owusu, Ergang Wang,* and Elisabet Ahlberg*

A quaternary amine-functionalized naphthalene diimide (NDI) moiety is synthesized and considered as a redox-active species for application in aqueous organic redox flow batteries. For the first time, this NDI is characterized electrochemically in aqueous solutions, using cyclic and rotating disk electrode voltammetry, bulk electrolysis, as well as ^{1}H-nuclear magnetic resonance (^{1}H-NMR) spectroscopy. The molecule reaches a solubility of 0.68 M in water and reversibly delivers two electrons at attractive potentials for flow battery applications. Further exploration with ^{1}H-NMR reveals a strong dimerization of the NDI species with an equilibrium constant of 146 M^{-1}. Using diffusion NMR coupled with rotating disk electrode voltammetry, it is shown that the dimer retains limited redox-activity, yielding two electrons per dimer unit. However, using galvanostatic bulk electrolysis, close to the theoretical capacity is obtained, indicating a fast dissociation reaction of the reduced dimer. Finally, the NDI species shows excellent stability; after constant cycling for 1 week, no degradation is detected. In conclusion, NDI is demonstrated to be a highly attractive candidate for aqueous redox flow batteries.

1. Introduction

There is a growing concern for Earth's ecological development over the last decades. In the list of actions to mitigate anthropological climate change, transitioning from the use of fossil fuels—which are known to make up for a majority of greenhouse gas emissions—to renewable energy sources is given considerable attention.[1–3] For this transition to be possible, large-scale energy storage is needed to bridge the intermittency of the sources,[2,4–7] and organic redox flow batteries (ORFBs) are often pointed out as prominent candidates for this application.[4,8–11]

For the redox active molecules in water-based systems, there is a set of conditions that must be fulfilled in order for the system to be competitive: The molecules need to be chemically stable at all states of charge (SOC), have a high solubility, have a reduction potential close to either extreme of the aqueous electrochemical stability window, be very cheap to produce, display electrochemical reversibility, fast electrode kinetics, and high diffusivity.[8,12–14] These conditions have led to the investigation of quinone-based materials[15–20] due to their widespread electrochemical use in both biological[21–23] and technological applications.[23–26] A well-performing flow battery with 9,10-anthraquinone-2,7-disulfonic acid (AQDS) coupled with HBr/Br$_2$ was seminally demonstrated in 2014,[27] and due to its fulfillment of many of the above criteria, AQDS has been thoroughly studied since and is often considered a model compound for aqueous ORFBs.[28–31] However, AQDS in its oxidized form has been shown to self-associate in solution, forming a redox-inactive dimer that somewhat impedes its use in electrochemical applications.[24,32]

1,4,5,8-naphthalenetetracarboxylic diimides have received much research attention due to their ability to form n-type semiconductor materials[33,34] and are heavily utilized as acceptor materials in polymer solar cells.[34–36] Typically, the electronic properties of napthalene diimides (NDIs) can be tuned by adding either electron-donating or electron-withdrawing groups to the naphthalene core, whereas the solubility is modified by substitution on the imide nitrogens.[37] Although water-soluble NDI materials have been synthesized and extensively studied,[38–43] an electrochemical investigation of NDIs in aqueous systems has not yet been reported. Furthermore, they have not previously been considered for aqueous flow battery applications.

In this work, in the pursuit of attractive candidates for ORFBs, an easily synthesized, highly water-soluble NDI molecule with a quaternary amine sidechain is electrochemically characterized and tested for its applicability in aqueous ORFB systems using cyclic voltammetry (CV), bulk electrolysis (BE), rotating disk electrode (RDE) voltammetry, and diffusion nuclear magnetic

C. Wiberg, F. Owusu, Prof. E. Wang
Applied Chemistry
Chalmers University of Technology
412 96 Gothenburg, Sweden
E-mail: ergang@chalmers.se

Prof. E. Ahlberg
Department of Chemistry and Molecular Biology
Gothenburg University
412 96 Gothenburg, Sweden
E-mail: elisabet.ahlberg@gu.se

The ORCID identification number(s) for the author(s) of this article can be found under https://doi.org/10.1002/ente.201900843.

**ADVANCED
SCIENCE NEWS**
www.advancedsciencenews.com

Energy Technology
Generation, Conversion, Storage, Distribution
www.entechnol.de

resonance (NMR). The molecule is simply referred to as NDI in this article.

2. Results and Discussion

To make NDI water-soluble at higher pH, the material was dissolved in chloroform through which chloromethane was bubbled, after which the pure NDI with quaternary amine sidechains precipitated out of solution. It should be noted that the last reaction step was only done for analytical purposes and is not necessary in the device application. At pH values below 8.1, which is a likely condition for the actual flow battery operation, the amine sidechains will be protonated, yielding solubilizing positive charges to the molecule without methylation. The solubility of the NDI was tested and found to be 0.68(2) M in deionized water at room temperature. The facile synthesis route shows promise for the material to be produced at low cost and low environmental harm.[44]

2.1. Cyclic Voltammetry

NDI displayed reversible redox processes in both acidic and neutral pH at potentials appreciably below that of the archetypical ORFB candidate, 2,7-AQDS,[30,32] see **Figure 1**. Increasing the scan rate does not significantly change the reduction potentials fo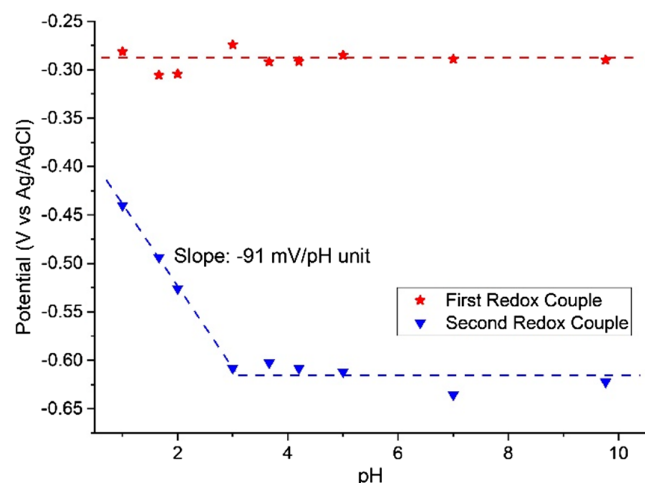r either the acid or neutral systems, indicating fast electron-transfer kinetics. As the concentration is increased at neutral pH, see Figure 1d, the first peak moves in the positive direction, and the second peak in the negative direction, terminating with a potential separation of almost 0.6 V. This might make the molecule attractive for use as both the negative and positive electrolytes in a symmetric flow battery setup.

The CV at pH 0 shows two reversible redox couples at roughly the same potential. At higher pH values, the second, more negative redox couple moves to more negative potentials, leaving behind a peculiarly broad one-electron redox couple whose position does not change with pH. The overlapping of the peaks at pH 0, as well as the broadness of the first redox couple at pH 7, makes analysis complicated, and to facilitate the reading of reduction potentials, simulations using the EC-Labs software from BioLogic were used, see Section 1 in Supporting Information. At pH values above 3, the second redox couple loses the pH dependence, reaching a reduction potential of −0.63 versus Ag/AgCl, see **Figure 2**. The slope of the lower pH-region of the potential—pH diagram for the second redox couple is −91 mV per pH unit, indicating a two electron, three proton relationship. This will be further discussed in the following sections. Figure 1 also shows that the peak separation of the redox couples is completely unaffected by sweep rate, indicating rapid electron transfer kinetics.

The thermodynamic reduction potential for the hydrogen evolution reaction (HER) is −0.21 and −0.62 V versus Ag/AgCl for the acidic and neutral electrolytes, respectively, placing it at
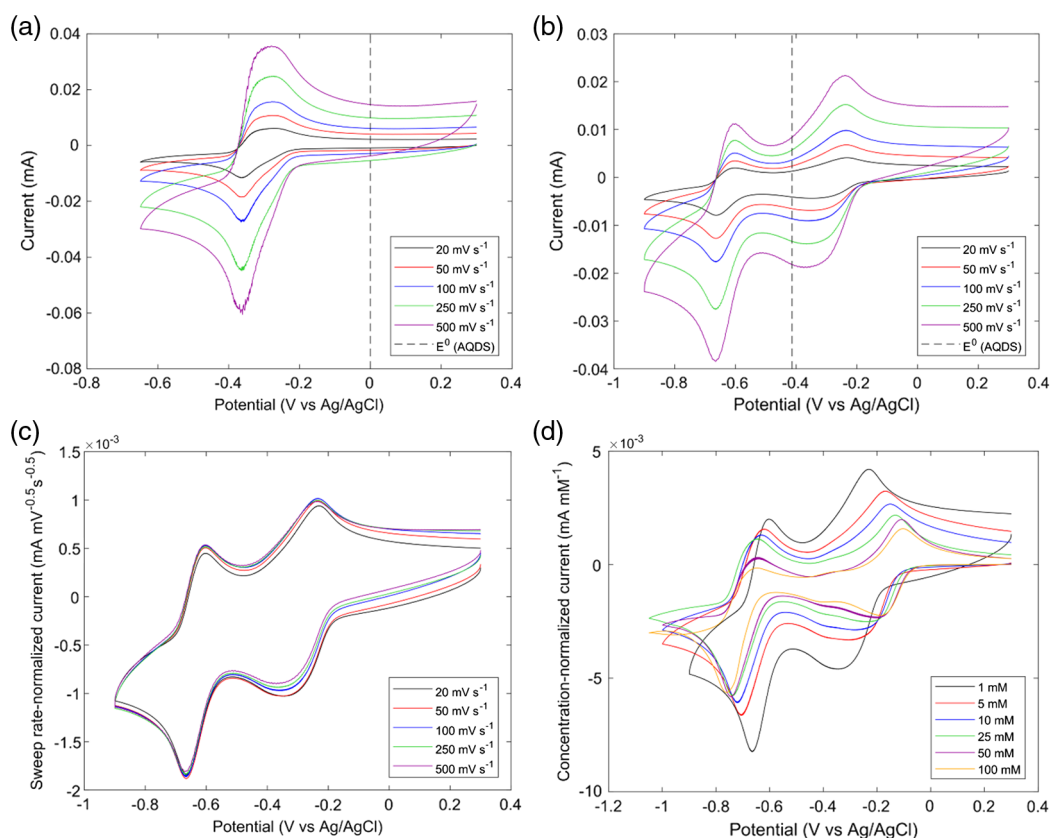
Figure 1. CV for 1 mM NDI in a) 1 M H_2SO_4 and b) pH 7 phosphate buffer. The dashed lines indicate the E^0 values for 2,7-AQDS, as a point of reference. c) Sweep rate-normalized CVs for 1 mM NDI in pH 7 phosphate buffer. d) Concentration-normalized CVs for different concentrations of NDI in pH 7 phosphate buffer, sweep rate = 20 mV s^{-1}.

ADVANCED
SCIENCE NEWS
www.advancedsciencenews.com

Energy Technology
Generation, Conversion, Storage, Distribution
www.entechnol.de

Figure 2. Potential–pH diagram for NDI at a concentration of 1 mM.

more positive potentials than for the complete reduction of NDI, albeit less so in the neutral electrolyte. Although the kinetics of the HER is known to be sluggish on glassy carbon electrodes, the parasitic side reaction might lead to a decreased coulombic efficiency during operation, especially at higher current densities.[45–47]

2.2. NMR Self-Association Study

NDI is known to self-associate, giving rise to a concentration-dependent displacement of the chemical shift from NMR which can be related to an equilibrium constant.[40,48,49] To acquire the equilibrium constant for the system at pH 7, solutions of varying concentrations of NDI in 0.5 M sodium phosphate buffer in D_2O were prepared and analyzed with ^{1}H-NMR. The sodium salt of the common NMR reference compound, 3-(trimethylsilyl) propionic-2,2,3,3-d4 acid (TSP-D4) was added at a constant concentration to all samples to enable accurate determination of the chemical shifts.
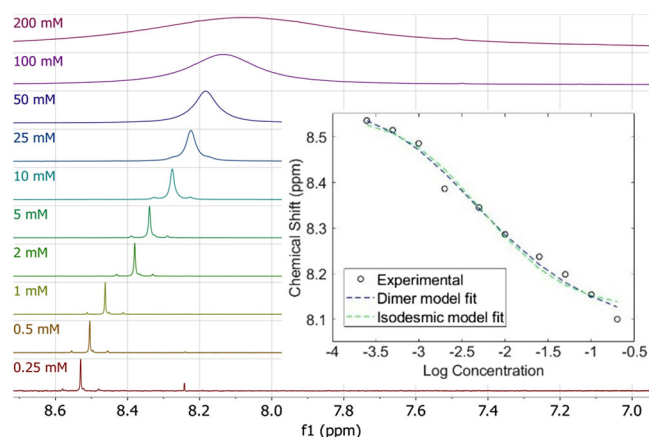
Figure 3. ^{1}H-NMR for NDI in pH 7 phosphate buffer in D_2O. The position of the aromatic peak is seen to broaden and move upfield at higher concentrations. The inset shows the fitting of the chemical shifts to the dimer and isodesmic models.

In **Figure 3**, the proton peak from the naphthalene core on NDI moves upfield at higher concentrations, clearly indicating self-association. This is supported by the peak broadening with concentration, which could be a result of the large amount of different conformations of NDI molecules in the sample population when self-aggregated or a decreased exchange rate between the monomer and the dimer species.[50,51] The peak shifts were fitted against two models, one where the NDI molecules only form dimers, the "dimer model," and one where they can also form larger oligomeric aggregates, the "isodesmic model."[40] The model expressions are found in Section 2 in Supporting Information, and the model fit is shown in the inset of Figure 3. The dimer and isodesmic models respectively yielded equilibrium constants of 146 and 104 M^{-1} and mean-squared errors of 3.9×10^{-4} and 6.8×10^{-4}.

The study of the self-association of NDI was further pursued using diffusion NMR. Diffusion coefficients for a range of concentrations of NDI in a sample of pH 7 phosphate buffer in deuterated water were collected, see **Figure 4**. As the diffusion coefficient decreases with increasing viscosity, the viscosities of all solutions were measured and used to acquire a set of viscosity-normalized diffusion coefficients, see Section 6 in Supporting Information for more information.

Due to the moderate decrease in diffusion coefficients with concentration, validity of the dimer model is assumed, and the measured diffusion coefficient is the fraction-weighted average of the diffusion coefficients for the monomer and the dimer.

$$D_{\text{measured}} = xD_{\text{monomer}} + (1 - x)D_{\text{dimer}} \quad (1)$$

where x is the molar fraction of monomer. From the equilibrium constant, the molar fractions of the monomer and dimer for each concentration were acquired, which in turn yielded an overdetermined system of equations. Using the least squares method, the system was solved for D_{monomer} and D_{dimer} for each viscosity used in the RDE analysis. The diffusion coefficients were then adjusted to compensate for the viscosity difference between the normal and deuterated solvents using the Stokes–Einstein equation, see Section 7 in Supporting Information and **Table 1**.
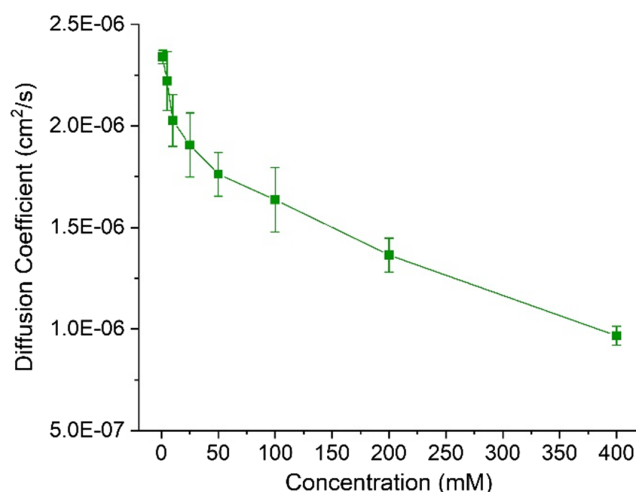
Figure 4. Diffusion coefficients for different concentrations of NDI measured by diffusion NMR.

Table 1. Diffusion coefficients for the monomer and dimer for NDI in pH 7 phosphate buffer solution.

Concentration [mM]	1	25	50
$D_{monomer}$ ($\times 10^{-6} cm^2 s^{-1}$)	2.0(0)	1.9(0)	1.9(0)
D_{dimer} ($\times 10^{-6} cm^2 s^{-1}$)	1.5(0)	1.4(0)	1.4(0)

2.3. RDE Voltammetry

Similar to what was seen for the CVs, the potential difference between the two reductions is significantly higher at the higher concentration. The diffusion-limiting currents were plotted against the square root of the rotation rate and showed linear relationships, see **Figure 5**. Interestingly, there are discrepancies between the Levich slopes for the first and the second electron transfers. For the case of 1 mM, the slope for the second electron is less steep than for the first one, whereas for 50 mM, it is steeper.

For the combined current for the first electron transfer of the monomer and the dimer, the slope of the Levich plot is given by combining the Levich equation for the respective species

$$i_l \omega^{-\frac{1}{2}} = 0.201 F A_{rde} \left(n_m C_m D_m^{\frac{2}{3}} + n_d C_d D_d^{\frac{2}{3}} \right) v^{-\frac{1}{6}} \tag{2}$$

where i_l is the diffusion-limited current (A), n the number of electrons, F is Faraday's constant (C mol^{-1}), A the geometrical electrode area (cm^2), C the concentration (mol cm^{-3}), D the diffusion coefficient (cm^2 s^{-1}), ω the rotation rate (rpm), and ν the
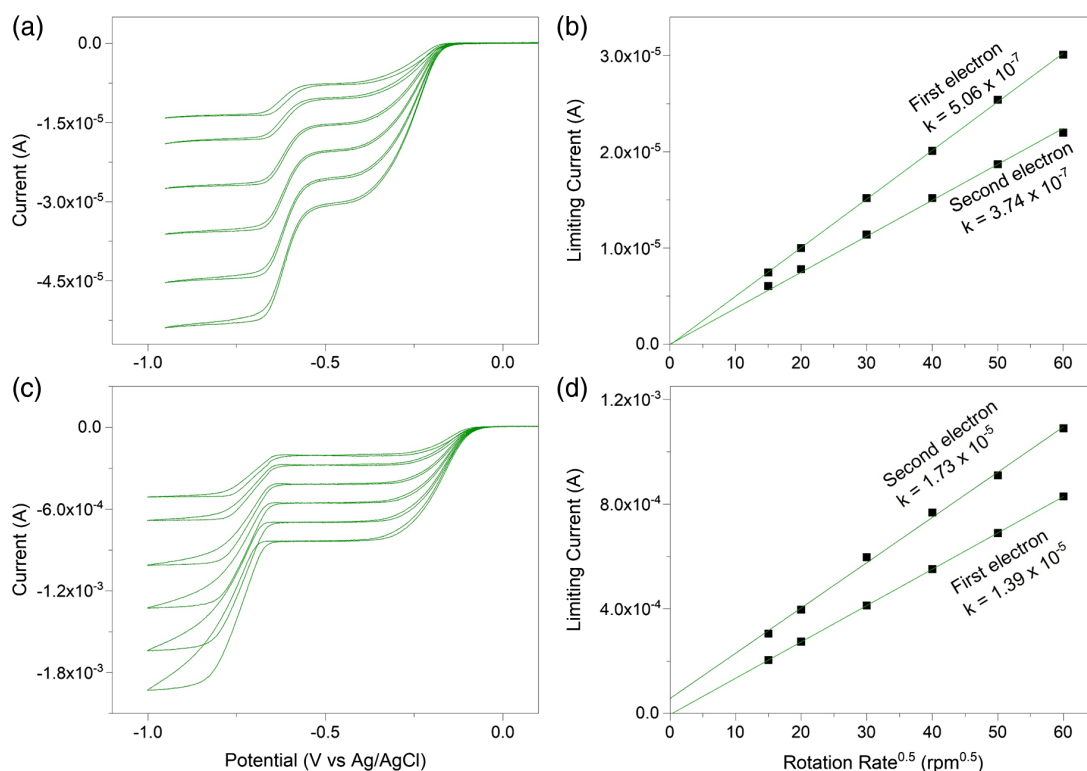
kinematic viscosity (cm^2 s^{-1}). The indices m and d denote the monomer and dimer, respectively. Although it was seen from the initial CV measurements that $n_m = 2$, inserting the diffusion coefficients acquired from diffusion NMR as well as the concentrations given by the equilibrium constant from ^{1}H-NMR gave the number of electrons for the reduction of the dimer, n_d. **Figure 6** shows the calculated Levich slopes for different values of n_d as well as the experimentally acquired values from RDE. The values acquired from RDE correspond well to the model where the dimer is reduced with one electron per dimer unit in the first electron wave. In other words, the dimer delivers half of the theoretical capacity during the first electron reduction.

Furthermore, the Levich plots for the second electron display subtle curvatures, as well as y-intercepts that are not zero. This is indicative of a CE-mechanism—perhaps the redox-limited dimer from the first reduction dissociates at a slow rate on the RDE time-scale, enabling further reduction through the provision of monomer.
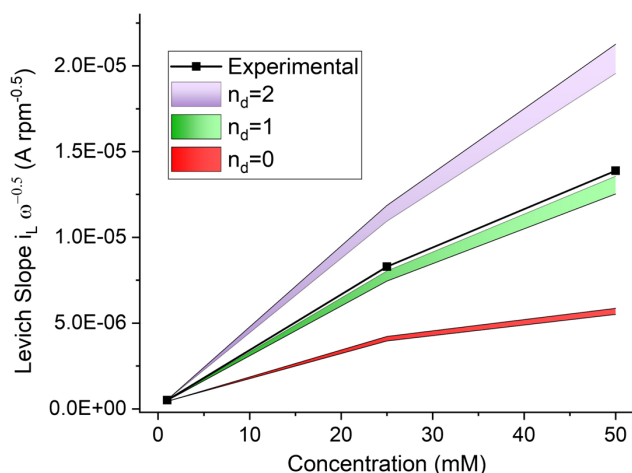
For the case of 1 mM NDI in the acid electrolyte, inserting the measured diffusion coefficient into the Levich equation together with $n = 2$ for both the monomer and the dimer gave good agreement with the limiting currents acquired experimentally. Ascertaining whether this is an indication of less self-association in the acid electrolyte or that the dimer retains full redox activity is not handled in this work.

2.4. Bulk Electrolysis

Based on the CVs, a pH of 6.4 was chosen for BE, which was considered a good compromise between keeping the reduction potential away from that of the HER while simultaneously


Figure 5. RDE for a) 1 mM and c) 50 mM NDI in buffer solution with corresponding b,d) Levich plots.

**ADVANCED
SCIENCE NEWS**
www.advancedsciencenews.com

Energy Technology
Generation, Conversion, Storage, Distribution

www.entechnol.de

Figure 6. Levich slopes for the first electron reduction of NDI in pH 7 buffer solution. The black line shows the experimentally acquired values, whereas the colored intervals depict the calculated values from Equation (2) with diffusion coefficients acquired from diffusion NMR and concentrations given by $K = 146\,\text{M}^{-1}$.

avoiding hydrolysis of NDI. However, as the NDI hydrolysis is reversible,[41,52] cycling at a higher pH might be beneficial to further avoid the HER.

In **Figure 7**a, both the reductive and oxidative curves have two plateaus, each corresponding to one of the two electron transfers. It is seen that the acquired reductive capacity reaches values close to the theoretical limit, as shown by the black dashed line. The oxidation reaches a slightly lower charge than the reduction, which in part is attributed to the parasitic HER. To minimize this effect in an actual flow battery, a variable reduction current should be used, applying higher currents at low SOC, and lower currents when the cell potential nears or surpasses that of hydrogen evolution. Apart from the effect of the HER, mass-transfer limitations as well as external oxidation mechanisms due to oxygen or light penetrating into the cell are other possible causes for the displayed disparity.
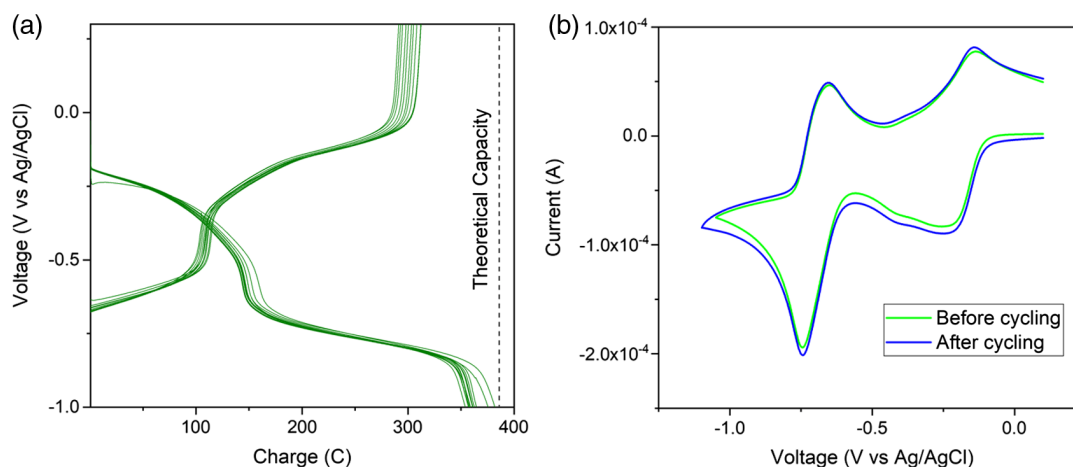
After the initial cycle, the cell was cycled 12 times at a constant current of 15 mA which corresponds to a charging/discharging speed of about 0.14 C, i.e., 7.14 h per cycle. Some capacity loss was seen between the first and the 12th cycle, which could be attributed to redox-active material diffusing through the glass frit into the counter electrode compartment. Figure 7b shows CVs for the NDI solution before the BE experiments started, as well as after the 12 cycles, through 1 week in time. No material degradation was observed, showing the extraordinary stability of NDI in the investigated system.

As mentioned in the previous section, the potential—pH diagram for the second reduction has a slope of $-91\,\text{mV}$ per pH unit, indicating a two electron–three proton relationship. However, since the RDE data at 1 mM in 1 M H_2SO_4, see Section 4 in Supporting Information, clearly shows that only two electrons are involved in the process, the only way the authors can explain the 91 mV per pH unit slope is that the two electrons and three protons per NDI molecule are shared by a self-associative dimeric structure as shown in **Figure 8**.

This would mean multiple different NDI dimers occurring simultaneously, and any relationship between them and the different oxidation states of the monomer is likely to be rather complex.
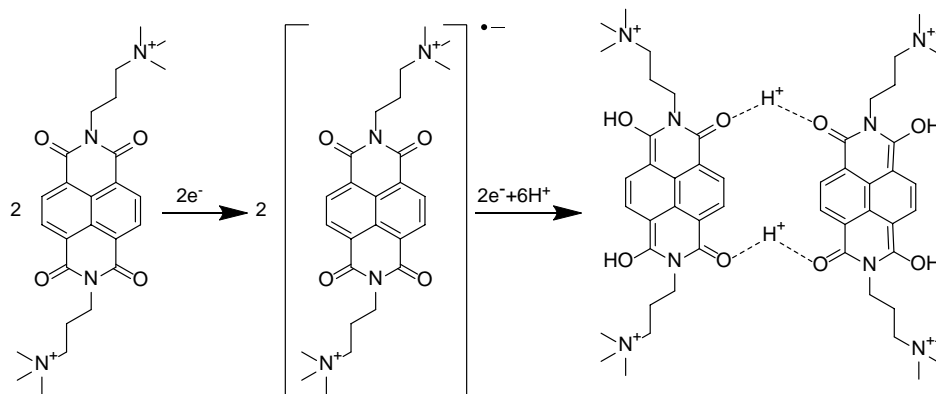
In short, the electrochemical behavior of NDI is rather complex, and some tendencies remain to be explained. The self-association of NDI seems to limit the reduction at short timescales, but as seen by the quite complete reduction of NDI by BE, this limit is nearly completely removed at long timescales. Thus, the dimerization is unlikely to cause a significant decrease in accessed capacity in the application of redox flow batteries.

3. Conclusion

A highly water-soluble NDI compound was synthesized with a high yield of 87% at a 70 g scale reaction. The facile synthesis route shows promise for the material to be produced at low cost and low environmental harm.

The molecule had two reversible redox couples at among the lowest potentials reported for materials considered for aqueous ORFBs. One of the couples was unaffected by pH, whereas the

Figure 7. a) 12 cycles of galvanostatic BE of a 25 mM NDI in pH 6.4 sodium phosphate buffer. The volume was 80 mL, and the current was 15 mA. b) CVs taken before and after the week-long cycling. NDI degradation was seen to be negligible.

**ADVANCED
SCIENCE NEWS**

www.advancedsciencenews.com

Energy Technology
Generation, Conversion, Storage, Distribution

www.entechnol.de

Figure 8. Proposed reduction mechanism for the NDI monomer at pH values below 3.

other couple showed a linear pH dependence at pH values below 3 with a slope of 91 mV per pH unit. The pH-dependence from CV, along with NMR and RDE studies all show a strong affinity for NDI to dimerize, and that the dimer formation affects the electrochemical behavior of the molecule. However, the molecule was readily reduced and oxidized during BE, as shown by the week-long cycling without any apparent degradation or change in the electrochemistry, making NDI a very promising candidate for redox flow battery applications.

4. Experimental Section

Synthesis of N,N′-Bis-[(3-Dimethylamino)Propyl]-1,4,5,8-Naphthalenetetracarboxylic Acid Diimide: (95 mL, 755 mmoL) of 3-(dimethylamino)-1-propylamine (Sigma Aldrich) was added to 500 mL of distilled water in a 1000 mL round-bottom flask and subjected to stirring.[53] 1,4,5,8-naphthalenetetracarboxylic acid anhydride (Sigma Aldrich) (50 g, 186 mmoL) was added portion-wise to the solution, at a temperature of 0 °C. The solution was left stirring under nitrogen, while slowly reaching room temperature. After 40 h, the mixture was filtered and washed with water, yielding 87% of the product as a pale, yellow powder.

^{1}H NMR (400 MHz, Chloroform-*d*) δ 8.76 (s, 4H), 4.31–4.22 (m, 4H), 2.44 (t, $J = 7.1$ Hz, 4H), 2.23 (s, 12H), 1.92 (tt, $J = 9.3$, 6.4 Hz, 4H); ^{13}C NMR (101 MHz, Chloroform-*d*) δ 198.88, 162.84, 135.47, 130.89, 126.64, 57.21, 45.38, 39.36, 25.98.

Synthesis of N,N′-Bis-[(3-Trimethylamino)Propyl]-1,4,5,8-Naphthalenetetracarboxylic Acid Diimide: Five grams of the material acquired in the previous step was dissolved in 100 mL of chloroform through which excess chloromethane was bubbled.[53] Material started precipitating after 30 min of stirring. The solution was left at room temperature overnight before the mixture was filtered and dried, affording a quantitative amount of the off-white product.

^{1}H NMR (400 MHz, deuterium oxide) δ 8.41 (s, 4H), 4.09 (t, $J = 7.0$ Hz, 4H), 3.44–3.35 (m, 4H), 3.02 (s, 18H), 2.20–2.07 (m, 4H); ^{13}C NMR (101 MHz, deuterium oxide) δ 163.88, 130.96, 125.86, 125.81, 64.00, 52.88, 37.63, 21.34.

General Voltammetry: Before starting each experiment, the 3 mm diameter glassy carbon working electrode (from BASi for CV and from Gamry for RDE) was polished with 0.3 μm alumina (Struers AP-D Suspension), rinsed with DI water, and then sonicated for 1 min in DI water. A platinum mesh was used as a counter electrode and Ag/AgCl in 3 M NaCl as reference electrode (BASi). All experiments were run in triplicate.

Cyclic Voltammetry: Cyclic voltammograms over a pH range between 0 and 9.76 were collected. For pHs 0 and 1, 1 and 0.1 M solutions of H_2SO_4 were used, and between pH 1.66 and 5, a Britton–Robinson Universal buffer was used.[54] For the universal buffer, to minimize weighing errors,

a 1 mM stock solution of NDI was made and titrated with 1 M NaOH to the desired pH values. The concentration change due to the added NaOH was considered negligible. For pH 7, a 0.5 M sodium phosphate buffer was used, and a 1 M sodium carbonate buffer was used for pH 9.76 . The CVs were collected in a random order with regard to pH. Voltammograms at scan rates of 20, 50 and 100, 250, and 500 mV s^{-1} were collected.

RDE Voltammetry: Rotation rates were chosen to 225, 400, 900, 1600, 2500, and 3600 rpm and the scan rate to 10 mV s^{-1}. The negative-going sweep for the first scan was chosen for analysis, and all experiments were done in triplicate. The supporting electrolyte solutions were 1 M H_2SO_4 and 0.5 M pH 7 sodium phosphate buffer.

Bulk Electrolysis: An 80 mL solution of 25 mM NDI in the neutral phosphate buffer, through which nitrogen gas was continuously bubbled, was reduced/oxidized on a reticulated vitreous carbon working electrode (BASi).

Nuclear Magnetic Resonance: All NMR spectra were recorded on a Varian 400 MHz spectrometer equipped with a Varian OneNMRProbe with a proton observe frequency of 399.95 MHz. All samples were measured in triplicate.

pH Measurements: pH measurements were performed using a Metrohm 827 pH lab pH-meter calibrated using buffer solutions (VWR) with pH = 12.00, 9.00, and 4.00.

Viscosity Measurements: Viscosity measurements were done using an Ubbelohde capillary (537 10/I and 531 01/0a) on a Schott AVS 360 viscometer and each measurement was repeated five times.

Solubility Testing: Solubility testing was done by preparing a saturated solution of NDI in water at room temperature, centrifuging the suspension at 12 500 rpm for 30 min and pipetting a volume of the supernatant into three separate vials. The vials were dried in a vacuum oven, and the dry weights were used for solubility calculations.

Supporting Information

Supporting Information is available from the Wiley Online Library or from the author.

Acknowledgements

Conflict of Interest

The authors declare no conflict of interest.

[1] N. S. Lewis, *MRS Bulletin* **2007**, *32*, 808.

[2] F. Pan, Q. Wang, *Molecules* **2015**, *20*, 20499.

[3] IEA, World Energy Outlook 2017, **2017**.

[4] S. E. Doris, A. L. Ward, A. Baskin, P. D. Frischmann, N. Gavvalapalli, E. Chenard, C. S. Sevov, D. Prendergast, J. S. Moore, B. A. Helms, *Angew. Chem. Int. Ed. Engl.* **2017**, *56*, 1595.

[5] A. A. Solomon, D. Bogdanov, C. Breyer, *Appl. Energy* **2019**, *235*, 1351.

[6] L. Bird, J. Cochran, X. Wang, *Wind and Solar Energy Curtailment: Experience and Practices in the United States* **2014**.

[7] A. Narayanan, K. Mets, M. Strobbe, C. Develder, *Renew. Energy* **2019**, *134*, 698.

[8] R. M. Darling, K. G. Gallagher, J. A. Kowalski, S. Ha, F. R. Brushett, *Energy Environ. Sci.* **2014**, *7*, 3459–3477.

[9] R. Ye, D. Henkensmeier, S. J. Yoon, Z. Huang, D. K. Kim, Z. Chang, S. Kim, R. Chen, *J. Electrochem. Energy Convers. Storage* **2017**, *15*, 010801.

[10] P. Leung, A. A. Shah, L. Sanz, C. Flox, J. R. Morante, Q. Xu, M. R. Mohamed, C. P. de León, F. C. Walsh, *J. Power Sources* **2017**, *360*, 243.

[11] K. Wedege, D. Bae, W. A. Smith, A. Mendes, A. Bentien, *J. Phys. Chem. C* **2018**, *122*, 25729.

[12] W. Wang, Q. Luo, B. Li, X. Wei, L. Li, Z. Yang, *Adv. Funct. Mater.* **2013**, *23*, 970.

[13] R. Dmello, J. D. Milshtein, F. R. Brushett, K. C. Smith, *J. Power Sources* **2016**, *330*, 261.

[14] R. Chen, *ChemElectroChem* **2018**, *6*, 603.

[15] D. P. Tabor, R. Gómez-Bombarelli, L. Tong, R. G. Gordon, M. J. Aziz, A. Aspuru-Guzik, *J. Mater. Chem. A* **2019**, *7*, 12833.

[16] J. Luo, W. Wu, C. Debruler, B. Hu, M. Hu, T. L. Liu, *J. Mater. Chem. A* **2019**, *7*, 9130.

[17] W. Liu, Y. Liu, H. Zhang, C. Xie, L. Shi, Y.-G. Zhou, X. Li, *Chem. Commun.* **2019**, *55*, 4801.

[18] M. Park, E. S. Beh, E. M. Fell, Y. Jing, E. F. Kerr, D. Porcellinis, M. A. Goulet, J. Ryu, A. A. Wong, R. G. Gordon, J. Cho, M. J. Aziz, *Adv. Energy Mater.* **2019**, *9*, 1900694.

[19] S. Jin, Y. Jing, D. G. Kwabi, Y. Ji, L. Tong, D. De Porcellinis, M.-A. Goulet, D. A. Pollack, R. G. Gordon, M. J. Aziz, *ACS Energy Lett.* **2019**, *4*, 1342.

[20] D. G. Kwabi, K. Lin, Y. Ji, E. F. Kerr, M.-A. Goulet, D. De Porcellinis, D. P. Tabor, D. A. Pollack, A. Aspuru-Guzik, R. G. Gordon, M. J. Aziz, *Joule* **2018**, *2*, 1894.

[21] I. Elmaci, M. A. Altinoz, *Biomed. Pharmacother.* **2016**, *83*, 635.

[22] J. Madeo, A. Zubair, F. J. S. Marianne, *SpringerPlus*, **2013**, *2*, 139.

[23] M. Aguilar-Martinez, N. A. Macias-Ruvalcaba, J. A. Bautista-Martinez, M. Gomez, F. J. Gonzalez, I. Gonzalez, *Curr. Org. Chem.* **2004**, *8*, 1721.

[24] T. J. Carney, S. J. Collins, J. S. Moore, F. R. Brushett, *Chem. Mater.* **2017**, *29*, 4801.

[25] M. Gómez, F. J. González, I. González, *J. Electrochem. Soc.* **2003**, *150*, E527.

[26] M. Gómez, F. J. González, I. González, *Electroanalysis* **2003**, *15*, 635.

[27] B. Huskinson, M. P. Marshak, C. Suh, S. Er, M. R. Gerhardt, C. J. Galvin, X. Chen, A. Aspuru-Guzik, R. G. Gordon, M. J. Aziz, *Nature* **2014**, *505*, 195.

[28] W. Lee, A. Permatasari, B. W. Kwon, Y. Kwon, *Chem. Eng. J.* **2019**, *358*, 1438.

[29] J. Cao, Z. Zhu, J. Xu, M. Tao, Z. Chen, *J. Mater. Chem. A* **2017**, *5*, 7944.

[30] C. Batchelor-McAuley, Q. Li, S. M. Dapin, R. G. Compton, *J. Phys. Chem. B* **2010**, *114*, 4094.

[31] L. Tong, Q. Chen, A. A. Wong, R. Gomez-Bombarelli, A. Aspuru-Guzik, R. G. Gordon, M. J. Aziz, *Phys. Chem. Chem. Phys.* **2017**, *19*, 31684.

[32] C. Wiberg, T. J. Carney, F. Brushett, E. Ahlberg, E. Wang, *Electrochim. Acta* **2019**, *317*, 478.

[33] H. E. Katz, A. J. Lovinger, J. Johnson, C. Kloc, T. Siegrist, W. Li, Y. Y. Lin, A. Dodabalapur, *Nature* **2000**, *404*, 478.

[34] P. Ledwon, D. Ovsiannikova, T. Jarosz, S. Gogoc, P. Nitschke, W. Domagala, *Electrochim. Acta* **2019**, *307*, 525.

[35] E. Ahmed, G. Ren, F. S. Kim, E. C. Hollenbeck, S. A. Jenekhe, *Chem. Mater.* **2011**, *23*, 4563.

[36] N. Zhou, A. Facchetti, *Mater. Today* **2018**, *21*, 377.

[37] S. V. Bhosale, C. H. Jani, S. J. Langford, *Chem. Soc. Rev.* **2008**, *37*, 331.

[38] P. Rajdev, M. R. Molla, S. Ghosh, *Langmuir* **2014**, *30*, 1969.

[39] Q. Lin, L. Liu, F. Zheng, P.-P. Mao, J. Liu, Y.-M. Zhang, H. Yao, T.-B. Wei, *RSC Adv.* **2017**, *7*, 38458.

[40] M. S. Cubberley, B. L. Iverson, *J. Am. Chem. Soc.* **2001**, *123*, 7560.

[41] M. B. Kim, D. W. Dixon, *J. Phys. Org. Chem.* **2008**, *21*, 731.

[42] F. A. Tanious, S. F. Yen, W. D. Wilson, *Biochemistry* **1991**, *30*, 1813.

[43] E. J. Gabbay, R. DeStefano, C. S. Baxter, *Biochem. Biophys. Res. Commun.* **1973**, *51*, 1083.

[44] V. Dieterich, J. D. Milshtein, J. L. Barton, T. J. Carney, R. M. Darling, F. R. Brushett, *Transl. Mater. Res.* **2018**, *5*, 034001.

[45] F. Y. Chen, J. G. Liu, H. Chen, C. W. Yan, *Int. J. Electrochem. Sci.* **2012**, *7*, 3750.

[46] C.-N. Sun, F. M. Delnick, L. Baggetto, G. M. Veith, T. A. Zawodzinski, *J. Power Sources* **2014**, *248*, 560.

[47] L. Wei, T. S. Zhao, Q. Xu, X. L. Zhou, Z. H. Zhang, *Appl. Energy* **2017**, *190*, 1112.

[48] K. P. Nandre, S. V. Bhosale, K. V. S. Rama Krishna, A. Gupta, S. V. Bhosale, *Chem. Commun.* **2013**, *49*, 5444.

[49] V. Steullet, D. W. Dixon, *J. Chem. Soc. Perkin Trans. 2* **1999**, 1547.

[50] D. P. Frueh, *Prog. Nucl. Magn. Reson. Spectrosc.* **2014**, *78*, 47.

[51] A. T. Alexandrescu, K. Rathgeb-Szabo, *J. Mol. Biol.* **1999**, *291*, 1191.

[52] T. C. Barros, I. M. Cuccovia, J. P. S. Farah, J. C. Masini, H. Chaimovich, M. J. Politi, *Org. Biomol. Chem.* **2006**, *4*, 71.

[53] C. Sissi, L. Lucatello, A. Paul Krapcho, D. J. Maloney, M. B. Boxer, M. V. Camarasa, G. Pezzoni, E. Menta, M. Palumbo, *Biorg. Med. Chem.* **2007**, *15*, 555.

[54] H. T. S. Britton, R. A. Robinson, *J. Chem. Soc.* (Resumed) **1931**, 1456.